1623 (2020) 012003 doi:10.1088/1742-6596/1623/1/012003

A Study of Low-Temperature Neutron Star Atmospheres.

A C Calder^{1,2}, P I Karpov^{3,4}, Z Medin⁴, and J M Lattimer¹

- ¹ Department of Physics and Astronomy, Stony Brook University, Stony Brook, NY 11794-3800, USA
- 2 Institute for Advanced Computational Science, Stony Brook University, Stony Brook, NY 11794-5250, USA
- Department of Astronomy & Astrophysics, UC Santa Cruz, Santa Cruz, CA 95064, USA
- ⁴ Los Alamos National Laboratory, Los Alamos, NM 87545, USA

E-mail: alan.calder@stonybrook.edu

Abstract. We present a study of how a low-temperature accreted atmosphere influences the emitted X-ray spectrum of a neutron star. The atmosphere models and spectra were computed with Zcode, a multigroup radiation transfer code developed at the Los Alamos National Laboratory. Though the underlying hot neutron star behaves as a blackbody, the atmosphere shifts the peak of spectrum away from a blackbody and toward higher energies, producing an emitted spectrum similar to a dilute blackbody. Quantifying the effects of this atmosphere will remove a source of uncertainty in X-ray observations and better constrain the mass-radius relation for neutron stars and thus the equation of state of dense matter. We present a suite of these atmospheres with varying compositions and temperatures as well as the resulting spectra.

1. Introduction

A significant unsolved problem in physics is the equation of state (EOS) of dense matter found in neutron stars, which are the stellar remnants formed by gravitational collapse supernovae. Only limited progress can be made from terrestrial experiments because they probe dense matter under conditions where there are nearly equal numbers of neutrons and protons and also extremely high temperatures. In contrast, the equilibrium state of dense matter in neutron stars is extremely neutron-rich and relatively cold. Information about these compact objects can be inferred from X-ray observations, pulsar timing, neutrinos coming from gravitational collapse supernovae, and, most recently, observations of gravitational radiation from neutron star mergers. In this contribution, we report on progress in modelling the effect of a low-temperature accreted atmosphere on the X-ray spectrum produced by a neutron star. We describe our methods, present preliminary spectra, and present a fitting formula for parameterizing spectra [1].

1.1. Neutron Stars

Neutron stars are the compact remnants of massive ($\approx 10-30~M_{\odot}$) stars that have undergone a core collapse supernova explosion. These objects are essentially pure neutron-rich nuclear matter that is confined by gravity and supported by the strong force (and neutron degeneracy). With a radius of approximately 11-13 km and a mass between 1.1 and 3.0 M_{\odot} [2], the objects

Content from this work may be used under the terms of the Creative Commons Attribution 3.0 licence. Any further distribution of this work must maintain attribution to the author(s) and the title of the work, journal citation and DOI.

1623 (2020) 012003

doi:10.1088/1742-6596/1623/1/012003

are relativistic and provide one of the most extreme environments in which matter may be found. Neutron stars are the locations of a variety of astrophysical phenomena, which lead to observations that can probe their properties, including

- thermal X-ray and optical emission from isolated and quiescent sources [3],
- X-ray bursts (XRBs) on neutron star surfaces [4],
- quasi-periodic oscillations (QPOs) from accreting neutron stars [5],
- periodic emissions from rapidly rotating X-ray pulsars with heterogeneous temperature distributions that can be studied via pulse-profile modeling [6], most recently with NICER [7],
- transient cooling following accretion episodes in quiescent stars that probes thermal properties of the crust and core [8],
- X-ray periodicities observed in flares from so-called soft gamma-ray repeaters that can be studied using neutron star seismology [9],
- pulsar glitches that constrain properties of neutron star crusts including superconductivity [10],
- spin-orbit coupling, observable through pulsar timing in extremely compact binaries, leading to measurements of moments of inertia [11],
- pulsar mass measurements [12, 13],
- neutrino signals from proto-neutron stars formed in relatively close galactic supernova [14], and
- gravitational radiation from merging neutron stars, leading to estimates of their extremely radius-sensitive tidal deformabilities [15] and possible production of the r-process responsible for half the heavy elements [16].

A neutron star is divided in to five major regions: inner and outer cores, crust, envelope, and atmosphere. The envelope and atmosphere have negligible mass, but are important for shaping the emergent spectrum as we will see. The envelope/atmosphere boundary is defined as the point where the material begins to become optically thin – specifically, where it is optically thin for high-energy X-ray photons, as described in Equation (12) of this paper. In the atmosphere, photons interact with matter through scattering and absorption; absorption softens the spectrum from a purely dilute blackbody and, depending on composition and temperature, can create lines. For example, one of the best fits for the spectrum of the neutron star in Cassiopeia A is a carbon atmosphere at $T_{\rm eff}=1.8\times10^6$ K, which has an absorption edge at $h\nu=0.35$ keV [17].

While there is currently no observational evidence for non-magnetic absorption features in neutron star spectra – as opposed to ion cyclotron lines caused by intense surface magnetic fields, which have been observed – these features tend to be at low photon frequencies and may therefore be obscured by gas and dust. Line broadening by magnetic fields, to such an extent that the spectral features cannot be observed, may also play a role for these objects [e.g., 18].

The crust is dense matter composed of nuclei (in β -equilibrium for example) and the composition is fixed or frozen out. As the density increases with depth, the nuclei of the crust form a lattice. Going deeper the density in the inner crust approaches neutron drip, $4\times10^{11}\mathrm{g\,cm^{-3}}$, where the chemical potential for neutrons goes from negative to positive, meaning that neutrons are free to enter and leave a nucleus and the lattice becomes a mix of nuclei and a neutron fluid. Here the geometry becomes important and what were three-dimensional features may shift to thin cylinders or planes; this configuration is referred to as "nuclear pasta." At even higher densities, the lattice may invert and become a lattice of dense matter and voids. The outer core is thought to be a superfluid soup of nucleons, muons, and electrons, and the inner core may have exotic matter such as hyperons or Bose condensates (pions or kaons) or may be

1623 (2020) 012003

doi:10.1088/1742-6596/1623/1/012003

a mixed phase of hadronic and deconfined quark matter. The reader is referred to Figure 3 and the accompanying text of [19] for additional details.

The mass-radius relation for neutron stars is critical for constraining the EOS of dense matter. At present, we have masses for 67 neutron stars [20–22]. While the masses in binary neutron star systems in which one member is a pulsar can be determined with great precision, the most precisely measured high-mass neutron stars are found in binary systems with a white dwarf. There are three in particular: PSR J0740+6620 at $2.14^{+0.10}_{-0.09}~M_{\odot}$ [22], PSR J1614-2230 at $1.908 \pm 0.016~M_{\odot}$ [23, 24], and PSR J0348+0432 at $2.01 \pm 0.04~M_{\odot}$ [25].

The mass-radius relation is constrained by general relativity. That is, for a given mass, the radius must be larger than the Schwarzchild radius, $R = \frac{2GM}{c^2}$. The relation is also constrained by causality, $c_s \leq c$, which for the case of the maximally compact EOS, $P = \rho - \rho_0$, implies $R \leq 2.823\frac{GM}{c^2}$. Also, the assumption of maximum mass further constrains a region of M-R space on the high-mass, small-radius side [26]. On the low-mass side, the relation is constrained by the Kepler limit for breakup of a rotating star. Within these limits, however, there is a considerable range of M-R space that allows for a host of EOSs incorporating different physics. The reader is referred to Figure 2 and the accompanying text of [19] and Figures 2 and 3 and the accompanying text of [26] for additional detail. The upshot is that with precise measurements of mass, we also need precise radii from observations to constrain the EOS. Observations of X-ray binaries offer radii measurements, but there are uncertainties involved that this work seeks to ameliorate.

1.2. X-ray Binaries

Neutron stars are born very hot and, accordingly, may be observed in X-rays. If a nascent neutron star is isolated, it can cool enough to become invisible in X-rays in as little as 100,000 years. If the neutron star has a companion, however, mass can accrete from the companion and several processes serve to keep the neutron star hot (glowing in X-rays). Such a system is said to be an X-ray binary.

X-ray binaries can be classified by the mass of the companion into low (companion mass $< 1.0 \ M_{\odot}$), intermediate, and high mass ($> 10.0 \ M_{\odot}$) [27, and references therein]. In the case of low-mass X-ray binaries, the emission of the system is dominated by X-rays from the neutron star, making them ideal to be observed in that energy band. Conversion of gravitational binding energy into thermal energy during accretion can keep the neutron star hot and emitting, but the system can also vary in brightness due to thermonuclear explosions of the accreted material. These explosions are observationally classified as type I X-ray bursts, and during these the luminosity of the system increases by typically two orders of magnitude. Type I X-ray bursts have a rise time of seconds and then a longer decay as the neutron star surface cools; with this cooling the X-ray spectrum softens. These events repeat on time scales from hours to days, which serves to keep the surface of the neutron star very hot [28].

2. Neutron Star Atmospheres

In the configurations described above, e.g. low-mass X-ray binaries in either quiescent or bursting phases, the radiation emitted by the underlying neutron star may be well-approximated as an ideal blackbody. The blackbody nature of these objects is due in part to their very high temperatures. If the spectrum of this blackbody could be directly observed, it would be straightforward to calculate the radius of the neutron star from the observed flux (assuming the distance is known). With that and the mass obtained from the properties of the binary system, the mass-radius relation would be readily found. The process is complicated by the presence of the atmosphere and any intervening gas or dust. Here we consider effects of the atmosphere given the underlying neutron star emitting radiation as a blackbody.

1623 (2020) 012003 doi:10.1088/1742-6596/1623/1/012003

Considerable previous work has gone into modeling neutron star atmospheres. Very early work on the X-ray emission from an accreting neutron star was performed by Zel'dovich and Shakura [29], who noted that the "computed spectrum differs considerably from a Planck curve." Alme and Wilson [30] extended this calculation with a diffusive treatment of the radiation in the atmosphere and considered the role of instabilities. Zampieri et al. [31] extended the work of Alme and Wilson by considering very low accretion rates and found "that the resulting spectral distributions are significantly harder than a blackbody at the star effective temperature." London, Taam, and Howard [32] calculated a suite of model atmospheres at effective temperatures from $\log T_{\rm eff}({\rm K}) = 6.46$ to 7.54 and surface gravities $\log g_{\rm surf}({\rm cm\,s^{-2}}) = 14.0$ to 15.0. They similarly reported spectra "significantly differ from a blackbody radiating at the effective temperature." Romani [33] examined the effect of various surface compositions in a calculation with realistic opacities for temperatures of $\log T_{\rm eff}({\rm K}) = 5.0$ to 6.5. They found that for hydrogen and helium atmospheres, the flux of soft X-rays can be much greater than the blackbody value, but that high-Z compositions produce results similar to that of a blackbody. Rajagopal and Romani [34] continued this work with improved opacities and compared results to the case of a high magnetic field. [See 35, 36, for discussion of conditions under which atmospheres may be treated as nonmagnetic.] There is considerable recent work on neutron star atmospheres with differing temperatures and compositions [see 17, 36–40, and references

In the atmosphere, both electron scattering and absorption and emission of radiation by electrons and ions contribute to the opacity. It is the balance between these two classes of processes that determines the overall shape of the spectrum from the neutron star as mediated by the atmosphere. There are several processes that scatter or absorb photons. If the energy of the photon is significantly less than the rest energy of an electron, i.e. $h\nu \ll m_e c^2$, as is the case for most photons of a blackbody with $T < 10^7$ K, the photons scatter elastically and the radiation is coherent [41]. This is the case of Thomson scattering, the cross section of which does not depend on frequency. If the photon energy is at least a moderate fraction of the rest energy of the electron, $h\nu > 0.01m_ec^2$, as occurs for most photons of a blackbody with $T > 10^7$ K, energy can be transferred between the photon and the electron; the direction of energy transfer tends to be toward the electron's thermal peak (a few $k_B T$). This is the case of Compton scattering. Free-free absorption (inverse Bremsstrahlung) has a strong inverse-frequency dependence, $\kappa \propto \nu^{-3}$, so it is particularly important at lower frequencies. If the atmosphere is cool enough to not be fully ionized, bound-free and bound-bound absorptions also contribute to the opacity.

Electron scattering leads to the situation of higher-energy photons readily escaping from deeper layers of the atmosphere, which hardens the spectrum relative to what it would be if the atmosphere were a true blackbody [42, 43]. Specifically, the emergent spectrum has the same peak as the underlying blackbody spectrum of the neutron star, but the same flux as a blackbody at the temperature of the atmosphere ($T_{\rm eff}$), which is cooler than the underlying neutron star; i.e., the spectrum is a dilute blackbody, and this difference is described by a color correction factor [e.g., 44]. On the other hand, low-energy photons are preferentially absorbed and then remitted as a blackbody at the atmosphere temperature. This broadens and reddens the spectrum from a dilute blackbody. At the same time, the strong ν^{-3} frequency dependence of the free-free emission causes the atmosphere to cool very efficiently at low temperatures, such that the atmosphere temperature drops very quickly as a function of radius for low-temperature neutron stars [See Figure 2 of 32]. This efficient cooling is responsible for the large color correction factors found in low-temperature neutron stars. [See Section 4.2 and Figure 5 of 45, for more detail.]

If atmosphere temperatures are above $T_{\rm eff} > 10^7$ K (which does not occur for the results shown in this paper), Compton scattering redistributes flux from frequencies above the spectral peak to those below, reddening the spectrum and sharpening the peak; Compton scattering

1623 (2020) 012003

doi:10.1088/1742-6596/1623/1/012003

additionally reheats the outer layers of the atmosphere. We must also consider gravitational redshift corrections to the spectrum. However, for the low-temperature neutron stars modeled in this work, the atmospheres are very thin (see the next section). Under these conditions, redshift corrections can be ignored except as a constant factor used to translate spectra results from the point of view of an observer at the stellar surface to that of an observer at infinity [cf. 44].

3. Simulation Instrument

The atmosphere models and spectra we present here were constructed with Zcode [45], developed at the Los Alamos National Laboratory. Zcode models one-dimensional hydrostatic atmospheres with a material equation of state and transports radiation from the hot neutron star where it interacts with the atmosphere via absorption, emission, and scattering. The radiation transfer in Zcode is described by a choice of two methods. The first is a Monte Carlo scheme with Compton scattering and general relativistic radiation transport through spherically symmetric shells of varying gravitational potential [46–48] and the second method is a diffusion scheme with Thomson scattering and a thin-atmosphere approximation to general relativity that allows a less-expensive calculation that is valid in some limits, e.g. low temperatures. Our algorithm for the Monte Carlo scheme was described in detail in [45]; here we briefly describe our algorithm for the diffusion scheme.

The diffusion equations for radiation transfer are found by taking the first and second angular moments of the radiation transfer equation then closing the system in the Eddington (P1) approximation. The radiation is assumed to be diffusive. We also assume scattering is Thomson only. For a thin, plane-parallel atmosphere geometry we combine these assumptions to have

$$\frac{\partial u_{\nu}}{\partial t^*} + \frac{\partial F_{\nu}}{\partial r^*} = \rho \kappa_{\nu} \left[-cu_{\nu} + 4\pi B_{\nu}(T) \right] \tag{1}$$

and

$$F_{\nu} = -\frac{c}{3\rho\kappa_{\nu}^{\text{tot}}} \frac{\partial u_{\nu}}{\partial r^{*}} \,. \tag{2}$$

Here u_{ν} is the frequency-dependent radiation energy density, F_{ν} is the frequency-dependent radiation flux in the outward radial direction,

$$B_{\nu}(T) = \frac{2h\nu^3/c^2}{e^{h\nu/kT} - 1} \tag{3}$$

is the Planck function, and $\kappa_{\nu}^{\rm tot} = \kappa_{\nu} + \kappa_{\rm Th}$ is the total attenuation opacity with κ_{ν} the absorption opacity and $\kappa_{\rm Th}$ the Thomson scattering opacity. Also, here $t^* = t(1+z_{\rm surf})^{-1}$ and $r^* = r(1+z_{\rm surf})$ are "local" time and radial coordinates [e.g., 49, 50] with $1+z_{\rm surf} = \left(1-\frac{2GM}{c^2R}\right)^{-1/2}$ the redshift factor at the surface and M the neutron star (total) mass. Note that in deriving Equations (1) and (2) from the full, general-relativistic, radiation transfer equation we have ignored terms following from the change in redshift with radius. For the atmospheres considered here, with widths $\Delta r \lesssim 10^4$ cm, these terms are small. As in [45], we have also assumed that the mass of the atmosphere ($< 10^{-15}~M_{\odot}$) is much less than M, that the atmosphere pressure ($\sim 10^{16}~{\rm Ba}$) is much less than $Mc^2/4\pi r^3$ ($\sim 10^{35}~{\rm Ba}$), that local thermodynamic equilibrium holds in the atmosphere, and that the atmosphere density ρ and temperature T are symmetric in the non-radial directions. Equations (1) and (2) are solved along with the material energy equation

$$\rho c_V \frac{\partial T}{\partial t^*} = \int_0^\infty d\nu \, \rho \kappa_\nu \left[c u_\nu - 4\pi B_\nu(T) \right] \tag{4}$$

1623 (2020) 012003 doi:10.1088/1742-6596/1623/1/012003

and the hydrostatic balance equation

$$\frac{\partial P_{\text{gas}}}{\partial r^*} = -\rho g_{\text{surf}} + \frac{1}{c} \int_0^\infty d\nu \, \rho \kappa_{\nu}^{\text{tot}} F_{\nu} \,, \tag{5}$$

where $P_{\rm gas}$ is the (ideal) gas pressure and c_V is the specific heat of the coupled ion-electron gas. Zcode solves the diffusion and material energy equations using the "multifrequency-gray" method described in [51] and the implementation ignores Compton scattering and assumes infinite ion-electron coupling. Equations (1) and (2) are solved in terms of frequency groups rather than individual frequencies. The total radiation energy density u and flux F are given by

$$\frac{\partial u}{\partial t^*} + \frac{\partial F}{\partial r^*} = -\rho \kappa_u c u + \rho \kappa_P 4 \sigma T^4 \tag{6}$$

and the finite-difference equation

$$F_{i+1/2} = -\frac{c}{3} \frac{\lambda_{i+1,i+1/2}^{\text{tot}} u_{i+1} - \lambda_{i,i+1/2}^{\text{tot}} u_i}{r_{i+1}^* - r_i^*}$$
(7)

[cf. 51], with κ_u and κ_P representing local opacity averages over energy density and the Planck function, respectively, and $\lambda_{i,i\pm1/2}^{\rm tot}$ representing an opacity average across cells and over energy density, as described in [51]. In Equation (7) we have assumed that the simulation is divided up radially into cells; i + 1/2 is the index of the face between cells i and i + 1. For B(T) in Equation (6) we have used

$$\int_0^\infty d\nu \, B_\nu(T) = \frac{\sigma T^4}{\pi} \tag{8}$$

with σ the Stefan-Boltzmann constant. Similarly, in the multigroup formalism Equation (4) is given by

$$\rho c_V \frac{\partial T}{\partial t^*} = \rho \kappa_u c_u - \rho \kappa_P 4\sigma T^4.$$
 (9)

In each time step of a diffusion simulation, Zcode first solves the group-equivalent versions of Equations (1) and (2) for each group independently, using the value of T from the beginning of the time step. With the group energy densities u_g and group fluxes F_g thus obtained, it calculates κ_u , κ_P , and $\lambda_{i,i\pm 1/2}^{\rm tot}$ for each cell. It then solves Equations (6) and (7) coupled with Equation (9) to find u and T at the end of the time step [see 52]. Once the atmosphere is in quasi-radiative equilibrium, Zcode adjusts ρ in each cell to maintain hydrostatic balance. The entire procedure is repeated until steady state is reached. Note that while not explicitly enforced,

$$u = \sum_{g} u_g \equiv \int_0^\infty d\nu \, u_\nu \tag{10}$$

and

$$F = \sum_{q} F_{g} \equiv \int_{0}^{\infty} d\nu \, F_{\nu} \tag{11}$$

in equilibrium, due to Equations (1), (2), (6) and (7).

Diffusion simulations use opacities from the LANL OPLIB database, which accounts for freefree, bound-free, and bound-bound transitions in local thermodynamic equilibrium [see 45, 53, for more detail]. The simulations used a spatial grid of 100 cells up to optical depth 10^4 and 300 logarithmically spaced frequency groups in the range $h\nu = 0.1$ eV to 100 keV, which is large enough to include the spectral peaks and frequencies two orders of magnitude on either side of

1623 (2020) 012003 doi:10.1088/1742-6596/1623/1/012003

the peaks for the model presented here. The optical depth upper limit is large enough that the thermal equilibrium condition

$$\sqrt{\tau_{g,\text{base}}\tau_{g,\text{base}}^{\text{tot}}} \gg 1$$
, (12)

where $\tau_{g,\text{base}}$ is the (group-dependent) absorption-only optical depth at the base of the atmosphere and $\tau_{g,\text{base}}^{\text{tot}}$ is the absorption-plus-scattering optical depth [54], holds for all frequency groups and temperatures considered [cf. 44, 45]. Therefore, the intensity of the radiation field at the inner boundary of the simulation is assumed to be isotropic and given by a Planck function at the same temperature as the base of the atmosphere, T_{base} . At the outer boundary, we use the Milne-Eddington vacuum condition

$$F_{g,\text{surf}} = \frac{cu_{g,\text{surf}}}{2}$$
 and $F_{\text{surf}} = \frac{cu_{\text{surf}}}{2}$. (13)

The parameters defining our models are the composition, which is assumed to be constant throughout the atmosphere, the effective temperature at the surface of the neutron star, and the surface gravity. Note, however, that the input temperature for simulations is actually $T_{\rm base}$, not $T_{\rm eff}$. For each model we guess a value for $T_{\rm base}$, run the simulation to steady state as described above, then adjust our guess based on the value of $T_{\rm eff}$ obtained and repeat until the model-specified $T_{\rm eff}$ is reached.

4. Preliminary Results

The model atmospheres we present here were originally presented in [1]. These atmospheres are for conditions that would be expected for quiescent (not bursting) low-mass X-ray binaries. "Standard" versions of low-mass X-ray binaries are thought to accrete hydrogen and ultra compact binaries helium or carbon; both types of accreting binaries are thought to have pure atmosphere compositions due to strong gravitational separation. Accordingly, the atmosphere models are composed of pure H, He, and C, each with effective temperatures of $5.3 \le \log T_{\rm eff}(K) \le 6.5$. All models were constructed with a surface gravity of $\log q_{\rm surf}({\rm cm\,s^{-2}}) = 14.0$.

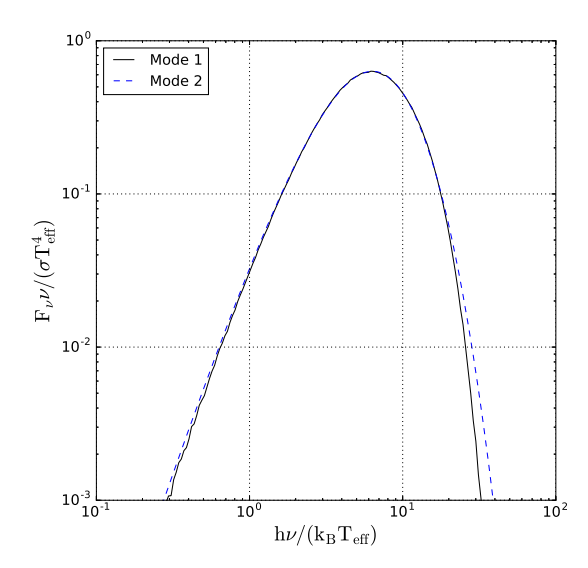
With Zcode, we first demonstrate the consistency between the Monte Carlo scheme with its more exact treatment of transport, scattering, and gravity and the simpler diffusion scheme, and then present model spectra calculated with the diffusion scheme. The left panel of Figure 1 presents normalized spectra for a model produced with the detailed Monte Carlo transport method (Mode 1) and a model produced with the diffusion scheme (Mode 2). The model for both is pure H, $\log T_{\rm eff}({\rm K})=6.5$ atmosphere, and the good agreement between the two spectra demonstrates the assumptions of the diffusion scheme are reasonable when compared to the more complete physics of the Monte Carlo method. These and subsequent spectra are presented as the normalized, frequency-dependent, outgoing surface flux $F_{\nu}/(\sigma T_{\rm eff}^4)$, as a function of normalized frequency $h\nu/(k_{\rm B}T_{\rm eff})$ with $k_{\rm B}$ the Boltzmann constant. We used the approximate expression

$$F_{\nu} \simeq F_q / \left(\nu_{q, \text{hi}} - \nu_{q, \text{lo}} \right) \,, \tag{14}$$

with $\nu_{g,\text{lo}}$ and $\nu_{g,\text{hi}}$ the low- and high-frequency boundaries of each group, to convert our group-dependent simulation fluxes to frequency-dependent values for plotting. Note that in contrast to the previous section, the models are now assumed to be in their equilibrium states such that the flux is constant through the thin atmosphere. Therefore, F_{ν} and F from here forward refer to their values at the surface, with the subscript "surf" dropped for convenience.

The right panel of Figure 1 and both panels of Figure 2 show the outgoing radiation spectra and the corresponding blackbody curves for our diffusion models of different compositions. Note that in the normalization scheme described earlier, all blackbody curves have the same normalized shape and amplitude regardless of $T_{\rm eff}$. As can be seen in the figures, the model

1623 (2020) 012003 doi:10.1088/1742-6596/1623/1/012003



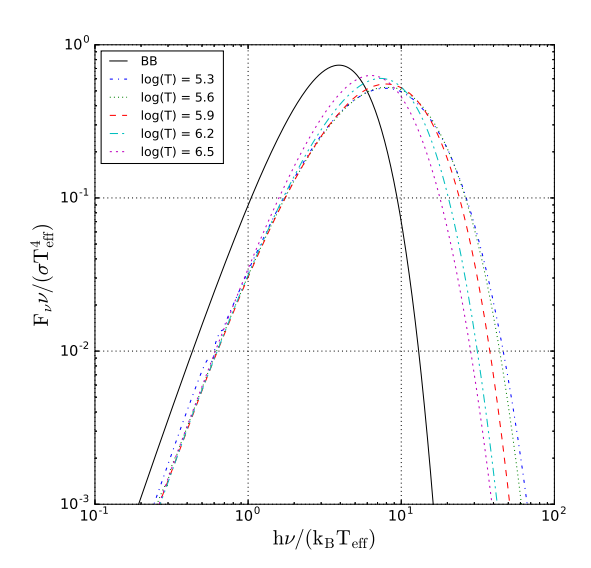


Figure 1. Left panel: Normalized spectra for a H atmosphere at $\log T_{\rm eff}({\rm K}) = 6.5$, calculated via Monte Carlo transport with Compton Scattering and general relativistic transport (Mode 1) and via diffusion and the assumption of a thin atmosphere (Mode 2). Right panel: Normalized spectra for H atmospheres over the range of temperatures simulated ($\log T_{\rm eff}({\rm K}) = 5.3-6.5$), calculated using the diffusion approximation. The gravity is constant at $\log g_{\rm surf}({\rm cm \, s}^{-2})$) = 14.0.

spectra differ significantly from those of blackbodies, despite the fact that the radiation intensity at the base of each atmosphere is Planckian.

The right panel of Figure 1, the pure H atmosphere, shows the evolution of the spectra with temperature. At the temperature increases, the spectra move closer to that of the underlying BB, i.e., the distribution narrows and the peak moves to lower energy. Overall, the spectra are smooth, with the exception of a minor absorption feature at $h\nu \sim 10$ eV $(h\nu/(k_{\rm B}T_{\rm eff}) \sim 0.6)$ for the lowest-temperature (log $T_{\rm eff}({\rm K})=5.3)$ model.

In the left panel of Figure 2, the pure He atmosphere, we see a similar situation. The spectra are mostly smooth and approach that of the BB at higher temperature, as in the case of H atmospheres. However, for the lowest-temperature model (log $T_{\rm eff}({\rm K})=5.3$), the spectrum contains significant absorption features for $h\nu \lesssim 70$ eV $(h\nu/(k_{\rm B}T_{\rm eff})\lesssim 4)$.

The right panel of Figure 2 presents the pure C atmospheres. Here the spectra are quite "bumpy" due to absorption effects. Note that while

$$\int_0^\infty d\nu \, F_\nu = \sigma T_{\text{eff}}^4 \tag{15}$$

for all of the spectra (in equilibrium), there is no restriction on the value of $F_{\nu}\nu/\left(\sigma T_{\text{eff}}^{4}\right)$; this quantity can and does exceed unity for a range of frequencies in several carbon atmosphere models with strong absorption features.

Note that the general trend of the spectra in Figures 1 and 2, that they move farther from the underlying BB as the atmosphere temperature decreases, agrees with results from previous studies [32, 44] and can be understood as efficient cooling that occurs in low-temperature atmospheres (Section 2).

1623 (2020) 012003 doi:10.1088/1742-6596/1623/1/012003

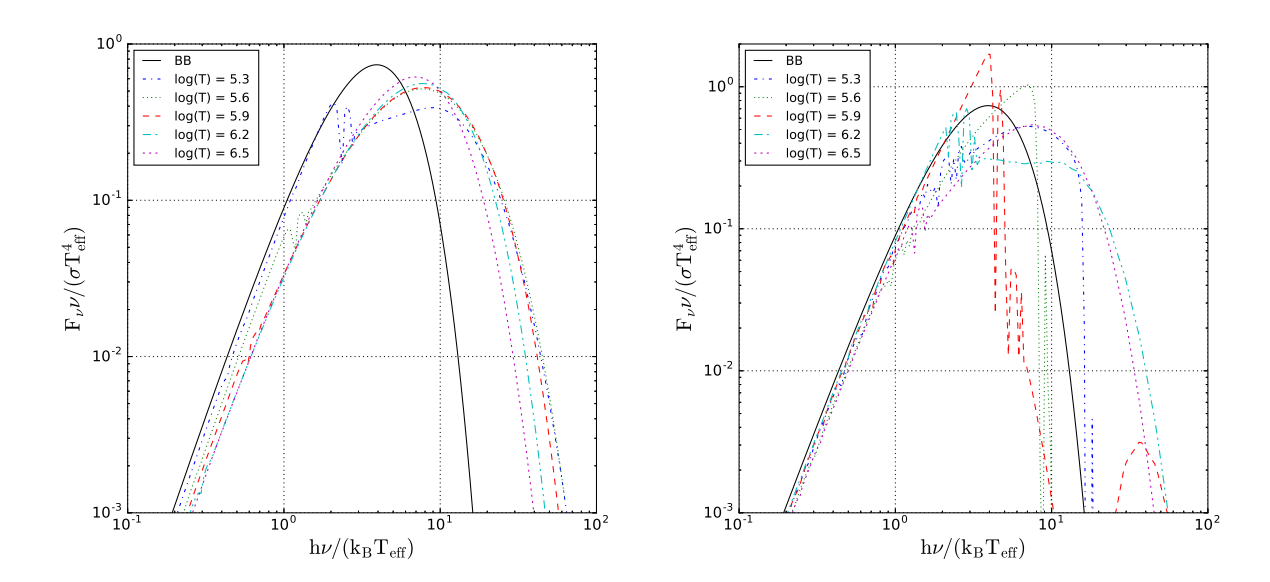


Figure 2. Normalized spectra for He (left panel) and C (right panel) atmospheres over the range of temperatures simulated ($\log T_{\rm eff}({\rm K}) = 5.3$ –6.5), calculated using the diffusion approximation. The gravity is constant at $\log g_{\rm surf}({\rm cm\,s^{-2}})) = 14.0$.

5. Model Fits

Model atmospheres can be used to calculate the radius of a neutron star, if the distance to the star is known. There are many difficulties associated with this process, some of which are outlined in [44, 55]. For the purposes of the current paper, we simply demonstrate here how differences in models can lead to large differences in the radius calculated from the models. To do this we construct fits to our models of the "hydrogenic" form [see 55, and references therein]

$$F_{\nu}^{\text{fit}}(T_{\text{eff}}) = \alpha \nu^3 \left[e^{\beta \{h\nu/(k_{\text{B}}T_{\text{eff}})\}^p} - 1 \right]^{-1}$$
 (16)

Here T_{eff} is the effective temperature of the atmosphere while α , β , and p are fit parameters. For our fits, as with our models, we are constrained by the normalization Equation (15).

There are two characteristic temperatures associated with the neutron star spectrum. The effective temperature $T_{\rm eff}$ is the temperature of a blackbody that produces the same total flux as the surface of the star whose spectrum we are trying to fit. We can imagine getting $T_{\rm eff}$ from a detector measuring the observed flux at Earth; but that also requires knowing the distance to the star and the radius of the star, and knowing about any material between us and the star. Note that since the radius of the star can't actually be observed, this is not a practical way of obtaining $T_{\rm eff}$, but it makes for a good thought experiment. The color temperature $T_{\rm c}$ is the temperature that produces a blackbody spectrum with a peak at the same frequency as the peak of the surface spectrum of the star.

If the true spectrum of the star is a blackbody, i.e., given by

$$F_{\nu}^{\mathrm{BB}}(T) = \pi B_{\nu}(T), \qquad (17)$$

then by definition $T_c = T_{\text{eff}} = T$ in Equation (17). Combining Equations (3) and (16) we have for the fit parameters $\beta = 1$, p = 1, and $\alpha = \alpha_{\text{BB}}$ with

$$\alpha_{\rm BB} = \frac{2\pi h}{c^2} \,. \tag{18}$$

1623 (2020) 012003

doi:10.1088/1742-6596/1623/1/012003

If instead the true spectrum is a dilute blackbody,

$$F_{\nu} = w F_{\nu}^{\mathrm{BB}}(T) \tag{19}$$

with w<1.0 the dilution factor, then by definition $T_{\rm c}=T$ in Equation (19), since $wF_{\nu}^{\rm BB}(T)$ and $F_{\nu}^{\rm BB}(T)$ have the same peak. From Equations (8) and (15) we have

$$wT_c^4 = T_{\text{eff}}^4. (20)$$

Combining Equations (16) and (19) we now have for the fit parameters $\beta = w^{1/4}$, p = 1, and $\alpha = w\alpha_{\rm BB}$.

Now suppose that we do not know the nature of the true spectrum, but we wish to calculate the radius by fitting the spectrum with both of the above models, the blackbody and the dilute blackbody. The simplest way we can fit the spectrum is by matching the spectral peak to the model peak, while ensuring that the normalization, Equation (15), holds. The observed flux F_{∞} , which is fixed and therefore constrains our models, is related to the flux at the surface $F = \sigma T_{\rm eff}^4$ by

$$F_{\infty} = \frac{L_{\infty}}{4\pi D^2} = \frac{R_{\infty}^2 \sigma T_{\text{eff}}^4}{D^2} \,, \tag{21}$$

where D is the distance to the star and

$$R_{\infty} = \frac{R}{1 + z_{\rm surf}} \tag{22}$$

is the apparent neutron star radius.

For the blackbody the model peak is at

$$h\nu_{\rm peak} = c_{\rm BB}k_{\rm B}T_{\rm eff}^{\rm BB}\,, (23)$$

with $c_{\rm BB} \simeq 2.82$ a constant; from Equation (21), then, we have

$$R_{\infty}^{\rm BB} = D\sqrt{\frac{F_{\infty}}{\sigma\{h\nu_{\rm peak}/(c_{\rm BB}k_{\rm B})\}^4}}.$$
 (24)

For the dilute blackbody the model peak is at

$$h\nu_{\rm peak} = c_{\rm BB}k_{\rm B}T_{\rm c}^{\rm dlt} \equiv \frac{c_{\rm BB}k_{\rm B}T_{\rm eff}^{\rm dlt}}{w^{1/4}},$$
 (25)

such that

$$R_{\infty}^{\text{dlt}} = D\sqrt{\frac{F_{\infty}}{w\sigma\{h\nu_{\text{peak}}/(c_{\text{BB}}k_{\text{B}})\}^4}}.$$
 (26)

Comparing Equations (24) and (26) we have

$$R_{\infty}^{\text{dlt}} = \frac{1}{\sqrt{w}} R_{\infty}^{\text{BB}} \quad \text{or} \quad R^{\text{dlt}} = \frac{1}{\sqrt{w}} R^{\text{BB}}.$$
 (27)

Therefore, for a given observed spectrum, a dilute blackbody model predicts a larger radius for the neutron star than a pure blackbody model does, by a factor of $1/\sqrt{w}$.

1623 (2020) 012003 doi:10.1088/1742-6596/1623/1/012003

6. Conclusions

We have presented preliminary results for a study of the emergent spectra from model neutron star atmospheres. We presented a verification test of consistency between the detailed Monte Carlo radiation transfer method and the diffusion scheme. The comparison showed reasonable agreement between modes.

The H spectra all resembled a dilute blackbody as expected. Accordingly, these spectra are smooth and may readily be fit by our "hydrogenic" model. For the case of the He atmospheres (left panel of Figure 2), the spectrum of the lowest-temperature model, $\log T_{\rm eff}({\rm K}) = 5.3$, contains significant absorption features for $h\nu \lesssim 70$ eV $(h\nu/(k_{\rm B}T_{\rm eff}) \lesssim 4)$. These features make finding a good fit with our "hydrogenic" model difficult. For all but the highest temperature, the pure C atmospheres (right panel of Figure 2) are similarly not smooth, making fits difficult. We thus conclude that there are limits on fits to the atmospheres of qLMXBs, and in particular, C atmospheres can't be readily fit.

Acknowledgments

This work was supported in part by the US Department of Energy under grant DE-FG02-87ER40317. Results in this paper were obtained using the high-performance computing system at the Institute for Advanced Computational Science at Stony Brook University. The authors thank Edward Brown for notes and several helpful discussions. The authors also thank the anonymous referee for thoughtful commentary that improved this manuscript.

References

- [1] Karpov P, Medin Z, Calder A and Lattimer J M 2016 American Astronomical Society Meeting Abstracts #227 (American Astronomical Society Meeting Abstracts vol 227) p 241 01
- [2] Lattimer J M 2017 Neutron stars are gold mines (In "Quarks, Nuclei and Stars: Memorial Volume Dedicated for Gerald E Brown" Holt, J. W. ed. World Scientific Publishing Co) pp 159–191
- [3] Mereghetti S 2011 *High-Energy Emission from Pulsars and their Systems* ed Torres D F and Rea N (Berlin, Heidelberg: Springer Berlin Heidelberg) pp 345–363 ISBN 978-3-642-17251-9
- [4] Lewin W H G, van Paradijs J and Taam R E 1993 Space Sci. Rev. 62 223–389
- [5] Miller M C 2006 Advances in Space Research 38 2680–2683
- [6] Leahy D A, Morsink S M, Chung Y Y and Chou Y 2009 ApJ **691** 1235–1242 (Preprint 0806.0824)
- [7] Arzoumanian Z, Bogdanov S, Cordes J, Gendreau K, Lai D, Lattimer J, Link B, Lommen A, Miller C, Ray P, Rutledge R, Strohmayer T, Wilson-Hodge C and Wood K 2009 astro2010: The Astronomy and Astrophysics Decadal Survey vol 2010 p 6 (Preprint 0902.3264)
- [8] Cackett E M, Wijnands R, Linares M, Miller J M, Homan J and Lewin W H G 2006 MNRAS 372 479-488 (Preprint astro-ph/0605490)
- [9] Samuelsson L and Andersson N 2007 MNRAS 374 256-268 (Preprint astro-ph/0609265)
- [10] Link B, Epstein R I and Lattimer J M 2000 Probing the neutron star interior with glitches (Astrophysics and Space Science Library vol 254) p 117
- [11] Lattimer J M and Schutz B F 2005 ApJ 629 979-984 (Preprint astro-ph/0411470)
- [12] Lattimer J M 2012 Annual Review of Nuclear and Particle Science **62** 485–515 (Preprint 1305.3510)
- [13] Ozel F and Freire P 2016 ARA&A 54 401–440 (Preprint 1603.02698)
- [14] Burrows A and Lattimer J M 1986 ApJ **307** 178–196

1623 (2020) 012003 doi:10.1088/1742-6596/1623/1/012003

- [15] Abbott B P, Abbott R, Abbott T D, Acernese F, Ackley K, Adams C, Adams T, Addesso P, R A, Goedhart S, Makhathini S, Oozeer N, Smirnov O M, Fender R P, Woudt P A and South Africa/MeerKAT S 2017 ApJ 848 L12 (Preprint 1710.05833)
- [16] Lattimer J M, Mackie F, Ravenhall D G and Schramm D N 1977 ApJ 213 225–233
- [17] Ho W C G and Heinke C O 2009 Nature **462** 71–73 (Preprint 0911.0672)
- [18] Suleimanov V F, Klochkov D, Pavlov G G and Werner K 2014 ApJS **210** 13 (Preprint 1311.6037)
- [19] Lattimer J M and Prakash M 2004 Science 304 536-542 (Preprint astro-ph/0405262)
- [20] 2019 stellarcollapse.org https://stellarcollapse.org/
- [21] Linares M, Shahbaz T and Casares J 2018 The Astrophysical Journal 859 54 URL https://doi.org/10.3847%2F1538-4357%2Faabde6
- [22] Cromartie H T, Fonseca E, Ransom S M, Demorest P B, Arzoumanian Z, Blumer H, Brook P R, DeCesar M E, Dolch T, Ellis J A, Ferdman R D, Ferrara E C, Garver-Daniels N, Gentile P A, Jones M L, Lam M T, Lorimer D R, Lynch R S, McLaughlin M A, Ng C, Nice D J, Pennucci T T, Spiewak R, Stairs I H, Stovall K, Swiggum J K and Zhu W W 2019 Nature Astronomy (Preprint 1904.06759)
- [23] Demorest P B, Pennucci T, Ransom S M, Roberts M S E and Hessels J W T 2010 Nature 467 1081–1083 (Preprint 1010.5788)
- [24] Arzoumanian Z, et al and NANOGrav Collaboration 2018 ApJ 859 47 (Preprint 1801. 02617)
- [25] Antoniadis J, Freire P C C, Wex N, Tauris T M, Lynch R S, van Kerkwijk M H, Kramer M, Bassa C, Dhillon V S, Driebe T, Hessels J W T, Kaspi V M, Kondratiev V I, Langer N, Marsh T R, McLaughlin M A, Pennucci T T, Ransom S M, Stairs I H, van Leeuwen J, Verbiest J P W and Whelan D G 2013 Science 340 448 (Preprint 1304.6875)
- [26] Lattimer J M and Prakash M 2016 *Physics Reports* **621** 127 164 ISSN 0370-1573 memorial Volume in Honor of Gerald E. Brown URL http://www.sciencedirect.com/science/article/pii/S0370157315005396
- [27] Tauris T M and van den Heuvel E P J 2006 Formation and evolution of compact stellar X-ray sources (In "Compact Stellar X-ray Sources" Lewin, W. H. G. and van der Klis, M. eds. Cambridge, UK: Cambridge University Press) pp 623–665
- [28] Bildsten L 2000 American Institute of Physics Conference Series (American Institute of Physics Conference Series vol 522) ed Holt S S and Zhang W W pp 359–369 (Preprint astro-ph/0001135)
- [29] Zel'dovich Y B and Shakura N I 1969 Soviet Ast. 13 175
- [30] Alme M L and Wilson J R 1973 ApJ **186** 1015–1026
- [31] Zampieri L, Turolla R, Zane S and Treves A 1995 ApJ 439 849-853 (Preprint astro-ph/9407067)
- [32] London R A, Taam R E and Howard W M 1986 ApJ **306** 170–182
- [33] Romani R W 1987 ApJ **313** 718–726
- [34] Rajagopal M and Romani R W 1996 ApJ 461 327 (Preprint astro-ph/9510094)
- [35] Zavlin V E, Pavlov G G and Shibanov Y A 1996 A&A 315 141–152
- [36] Potekhin A Y 2014 Physics Uspekhi 57 735-770 (Preprint 1403.0074)
- [37] Madej J, Joss P C and Różańska A 2004 ApJ **602** 904–912
- [38] Özel F 2013 Reports on Progress in Physics **76** 016901 (Preprint 1210.0916)

1623 (2020) 012003

doi:10.1088/1742-6596/1623/1/012003

- [39] Suleimanov V F, Klochkov D, Pavlov G G and Werner K 2014 ApJS 210 13 (Preprint 1311.6037)
- [40] Suleimanov V F, Poutanen J and Werner K 2018 A&A 619 A114 (Preprint 1808.10655)
- [41] Townsend R 2006 URL http://www.bartol.udel.edu/~owocki/phys633/14-opacity. pdf
- [42] Miller M C, Boutloukos S, Lo K H and Lamb F K 2011 Fast X-ray Timing and Spectroscopy at Extreme Count Rates (HTRS 2011) p 24 (Preprint 1105.2030)
- [43] Brown E 2019 "Stellar Astrophysics" freely available as part of the Open Astrophysics Bookshelf, URL http://www.pa.msu.edu/~ebrown/docs/stellar-notes.pdf
- [44] Suleimanov V, Poutanen J and Werner K 2011 A&A 527 A139 (Preprint 1009.6147)
- [45] Medin Z, von Steinkirch M, Calder A C, Fontes C J, Fryer C L and Hungerford A L 2016 ApJ 832 102 (Preprint 1611.09937)
- [46] Lindquist R W 1966 Annals of Physics **37** 487–518
- [47] Fleck Jr J A and Cummings Jr J D 1971 J. Comput. Phys. 8 313-342 ISSN 0021-9991 URL http://dx.doi.org/10.1016/0021-9991(71)90015-5
- [48] Canfield E, Howard W M and Liang E P 1987 ApJ 323 565–574
- [49] Thorne K S 1977 ApJ **212** 825–831
- [50] Ayasli S and Joss P C 1982 ApJ **256** 637–665
- [51] Winslow A M 1995 Journal of Computational Physics 117 262–273
- [52] Gittings M, Weaver R, Clover M, Betlach T, Byrne N, Coker R, Dendy E, Hueckstaedt R, New K, Oakes W R, Ranta D and Stefan R 2008 Computational Science and Discovery 1 015005 (Preprint 0804.1394)
- [53] Magee N H, Abdallah Jr J, Clark R E H, Cohen J S, Collins L A, Csanak G, Fontes C J, Gauger A, Keady J J, Kilcrease D P and Merts A L 1995 Astrophysical Applications of Powerful New Databases (Astronomical Society of the Pacific Conference Series vol 78) ed Adelman S J and Wiese W L p 51
- [54] Rybicki G B and Lightman A P 1986 Radiative Processes in Astrophysics (Wiley)
- [55] Lattimer J M and Steiner A W 2014 ApJ 784 123 (Preprint 1305.3242)